ISSN 1063-7729, Astronomy Reports, 2010, Vol. 54, No. 2, pp. 173–183. © Pleiades Publishing, Ltd., 2010.
Original Russian Text © M.V. Eselevich, 2010, published in Astronomicheskiĭ Zhurnal, 2010, Vol. 87, No. 2, pp. 197–208.

Detecting the Widths of Shock Fronts Preceding Coronal Mass Ejections

M. V. Eselevich

Institute of Solar-Terrestrial Physics, Siberian Branch, Russian Academy of Sciences, ul. Lermontova 126a, Irkutsk, 664033 Russia

Received August 19, 2009; in final form, September 10, 2009

Abstract—The perturbed zones and shocks preceding coronal mass ejections (CMEs) are studied using the data of the Mark 4, LASCO C2, and LASCO C3 coronagraphs. Detection of the perturbed zone indicating the presence or absence of the shock is most reliable in a frame moving with the frontal structure of the CME. The ability to correctly measure the width δ_F of the shock front using the Mark 4 and LASCO C2 data is established. The front width δ_F observed along the streamer belt at distances $R < 5\ R_\odot$ from the center of the Sun is of the order of the mean free path of protons. This means that the energy dissipation in the shock front is collisional at such distances. At distances $R \geq (10-15)\ R_\odot$, a new discontinuity with a front $\delta_F^* \ll \delta_F$ is formed in the leading portion of the front. Within the errors, $\delta_F^* \approx (0.1{-}0.2)\ R_\odot$ is independent of the distance R and is determined by the LASCO C3 spatial resolution. Initially, the discontinuity on the scale δ_F^* is weak and coexists with the front with width δ_F. The relative amplitude of this discontinuity increases and the brightness profile behind it flattens as long as the distance R increases. This transformation of the brightness profile from a front of width δ_F to a discontinuity of width $\delta_F^* \ll \delta_F$ is explained as a transition from a collisional to a collisionless shock.

DOI: 10.1134/S1063772910020101

1. INTRODUCTION

A rapid coronal mass ejection (CME) moving through the corona with a super-Alfvenic velocity should excite a preceding shock. This is supported by the type II radio bursts that frequently accompany CMEs [1]. A number of experiments [2–4] observing the plasma in the region following the assumed shock front have detected broadening of the ultraviolet OVI line associated with plasma heating that occurs due to the compression in the shock front. However, attempts over many years to relate the peculiarities observed in white-light coronal images directly to the shock have failed. Only long-term observations carried out by spacecraft coronagraphs with high sensitivities that have become available in recent years enable us to approach this goal [5]. An additional difficulty is that the CME frontal structure and the shock front have similar geometries and can have fairly close locations. MHD computations and the resemblance to bow shocks were used to identify shock fronts in coronal images in [6–8]. Another technique was used in [9, 10], namely, when the CME velocity u relative to the surrounding coronal plasma is below a certain critical velocity u_C, there is a leading perturbed zone extended along the direction of the CME propagation. When $u > u_C$, a discontinuity in the differential brightness or plasma density is formed in the leading portion of the perturbed zone. Since u_C approaches the local speed of the fast magnetoacoustic wave, which is approximately equal to the Alfven speed in the solar corona, the formation of such a discontinuity above u_C can be identified with the formation of the shock.

If we can identify the shock fronts in coronal images, we can determine the quantitative characteristics of the shocks. Among these characteristics, the width of the shock front δ_F is very important, since it indicates possible mechanisms for the energy dissipation. However, it is difficult to determine δ_F, due to the limited spatial resolution of coronagraphs and the effect of line-of-sight averaging in the optically thin corona. The goals of the present study are, first, to establish the correctness of δ_F measurements in the solar corona carried out using the modern Mark 4 and LASCO C2 coronagraphs and, second, to discuss a probable mechanism for the energy dissipation in the shock front indicated by measurements of the front width δ_F.

2. ANALYSIS METHOD

The coronal images obtained by the SOHO LASCO C2 and C3 coronagraphs [11] are presented in the form of the differential brightness $\Delta P = P(t) - P(t_0)$, where $P(t_0)$ is the unperturbed brightness

detected at a time t_0 preceding the event considered and $P(t)$ the brightness detected at a time $t > t_0$. We use the calibrated LASCO images with the total brightness $P(t)$ in units of the mean solar brightness (P_{MSB}).

The behavior of CMEs and their perturbed zones is studied using differential-brightness images. For this purpose, we use ΔP contours and construct both radial sections (extended along the solar radius) with fixed position angles PA and non-radial sections. In the plots, the distances from the center of the Sun are marked R, whereas the distances from the center, for example, of the frontal structure are marked r. All distances in the plots are expressed in units of the solar radius $R_\odot$. The position angles PA are measured counterclockwise from the north pole of the Sun.

For distances $1.2\ R_\odot < R < 2\ R_\odot$, we used images of the polarized brightness obtained by the Mark 4 ground coronagraph polarimeter (MLSO); these images were in the form of the differential brightness, quite similar to that of the LASCO data.

3. IDENTIFYING SHOCK FRONTS PRECEDING CMEs

When identifying a shock front, it is most reliable to trace its formation, which occurs at CME velocities $u > u_C$. This can be accomplished only in simple cases when the CME propagates near the plane of the sky and displays three distinct parts: the frontal structure (FS) surrounding a darker cavity and the bright core (this core, which is associated with the erupting filament, can be absent in some cases). The reliable identification of these CME parts enables investigation of the evolution of the perturbed zone and the formation of the shock using a frame moving with the frontal structure. Our analysis was carried out along the line of propagation of the CMEs, i.e., along the streamer belt.

Let us first determine the appearance in a frame moving with the frontal structure of a perturbed zone that precedes a CME that has a velocity $u < u_C$. One example is the ejection of May 7, 1997, which appeared in the LASCO C2 field of view at 10:26 UT (universal time is used everywhere below) in position angle PA $\approx 269°$ and had a velocity $V \approx 234$ km/s. Figure 1 (top) presents a differential-brightness image (in the form of contours) for 13:41, when the CME was in the LASCO C2 field of view. The CME frontal structure resembles a circle (schematically shown in Fig. 1 by the dashed arc marked FS). The CME perturbed zone is mainly a region of enhanced brightness that extends far in front of the CME.

We can see the time evolution of the perturbed zone in the differential brightness distributions $\Delta P(t, R) = P(t, R) - P(t_0, R)$ constructed along the direction of propagation of the CME (shown by the dashed line in the upper plot of Fig. 1) in detail. The differential brightnesses distributions $\Delta P(t, R)$ constructed in a frame moving with the frontal structure are presented in Fig. 1 (bottom). When constructing this plot, (1) each $\Delta P(t, R)$ was normalized to the maximum differential brightness $\Delta P_{\max}$ detected near the frontal structure; (2) all $\Delta P(t, R)$, except the earliest in time, are shifted along the distance R such that all the FS positions coincide. The FS region for 11:29 is approximately shown in the plot by slanted hatching. The boundaries of the frontal structure are shown by the $0.5\Delta P_{\max}$ differential-brightness level. The perturbed zone preceding the CME adjoins the leading boundary of the frontal structure.

The lower plot in Fig. 1 shows that the relative brightness (plasma density) in the perturbed zone increases with time. This probably describes the compression of the unperturbed (background) plasma located in front of the CME. The analysis of $\Delta P(t, R)$ constructed for the other position angles shows that there are nonlinear oscillations in brightness, in addition to brightness enhancements preceding the frontal structure. The most important feature of the perturbed zone preceding the CME, which has a velocity $u < u_C$, is the absence of any abrupt boundary in the leading portion of the zone. The formation of a discontinuity in the differential brightnesses of the leading portion of the perturbed zone preceding an ejection with a CME velocity $u > u_C$ enables us to identify this discontinuity with the shock preceding the CME [10]. Figure 2 presents an example of such an event. In this event (September 20, 1997, which first appeared in the LASCO C2 field of vision at 10:20, PA $\approx 272°$, $V \approx 777$ km/s), the CME contains three distinct parts. Figure 2 (three upper plots) presents contours of the differential brightness for three successive times corresponding to the CME motion observed in the LASCO C2 field of vision. The CME frontal structure is shown by the dotted arc.

The lower plot of Fig. 2 presents the differential brightnesses distributions $\Delta P(t, R)$ constructed for four successive times in a frame moving with the frontal structure. At the initial time (filled circles), there is virtually no perturbed zone preceding the frontal structure (which is shown by the slanted hatching). However, at the next time (hollow circles), we see a region of compressed plasma preceding the frontal structure, with this plasma being bounded from the front by the shock (crossed hatching). The shock moves faster than the frontal structure and successively becomes located farther and farther from the frontal structure (filled diamonds and triangles). On the contrary, the leading boundary of the bright core lags behind the frontal structure because of its lower velocity.

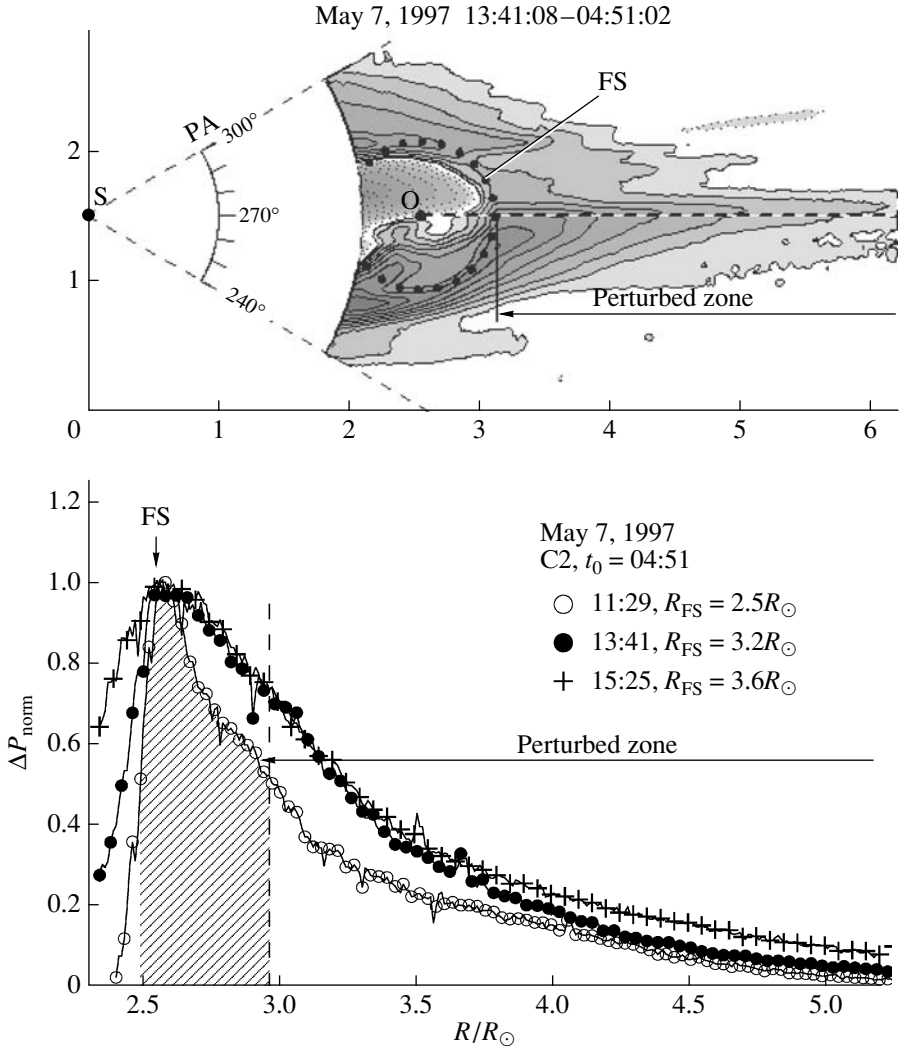

Fig. 1. CME observed on May 7, 1997 with no shock formation detected by the LASCO C2 data. Shown at the top is the differential-brightness image for 13:41. The point S indicates the center of the Sun. The dotted circle indicates the frontal structure (FS). Shown at the bottom are successive differential-brightness distributions constructed from the FS center in the direction indicated by the dashed line presented in the upper plot. The frame is moving with the frontal structure, and the distributions are normalized to the FS brightness detected at the initial time.

4. CURRENT SHEET DISTINGUISHED FROM THE SHOCK FRONT

Stationary irregularities of the plasma density in the corona (identified in coronal images as abrupt changes in brightness on small spatial scales) must contain current sheets. This is true because stationary plasma-density irregularities can be supported only by irregularities in the magnetic field, which requires electric currents on the same scales. Either collisions between electrons and ions or plasma instabilities result in an increase in the width of the current sheet, due to plasma diffusion across the magnetic field. However, current-sheet diffusion can be almost absent in rarefied high-temperature plasma. In this case, the width of the current sheet can remain of the order of the Larmor radius of the electrons ρ_e for a long time. The width of a stationary current sheet δ_I expanding due to collisions at time t can be estimated by the relation [12, p. 90]

$$\delta_I \approx \rho_e \sqrt{t/\tau_{ep}},$$

where τ_{ep} is the mean time between electron–proton collisions. The dependence of the time between collisions on the temperature and density in seconds can be expressed as $\tau_{ep} \approx 10^{-2} T^{3/2}/N$, with T in Kelvins and N in cm^{-3} [12, p. 54].

Let us estimate δ_I in the corona. Assuming for a distance $R \approx 2.1 R_\odot$ the plasma temperature $T \approx 1.4 \times 10^6$ K, magnetic field $B \approx 0.55$ G, and plasma density $N \approx 6 \times 10^6$ cm^{-3} [13], we obtain

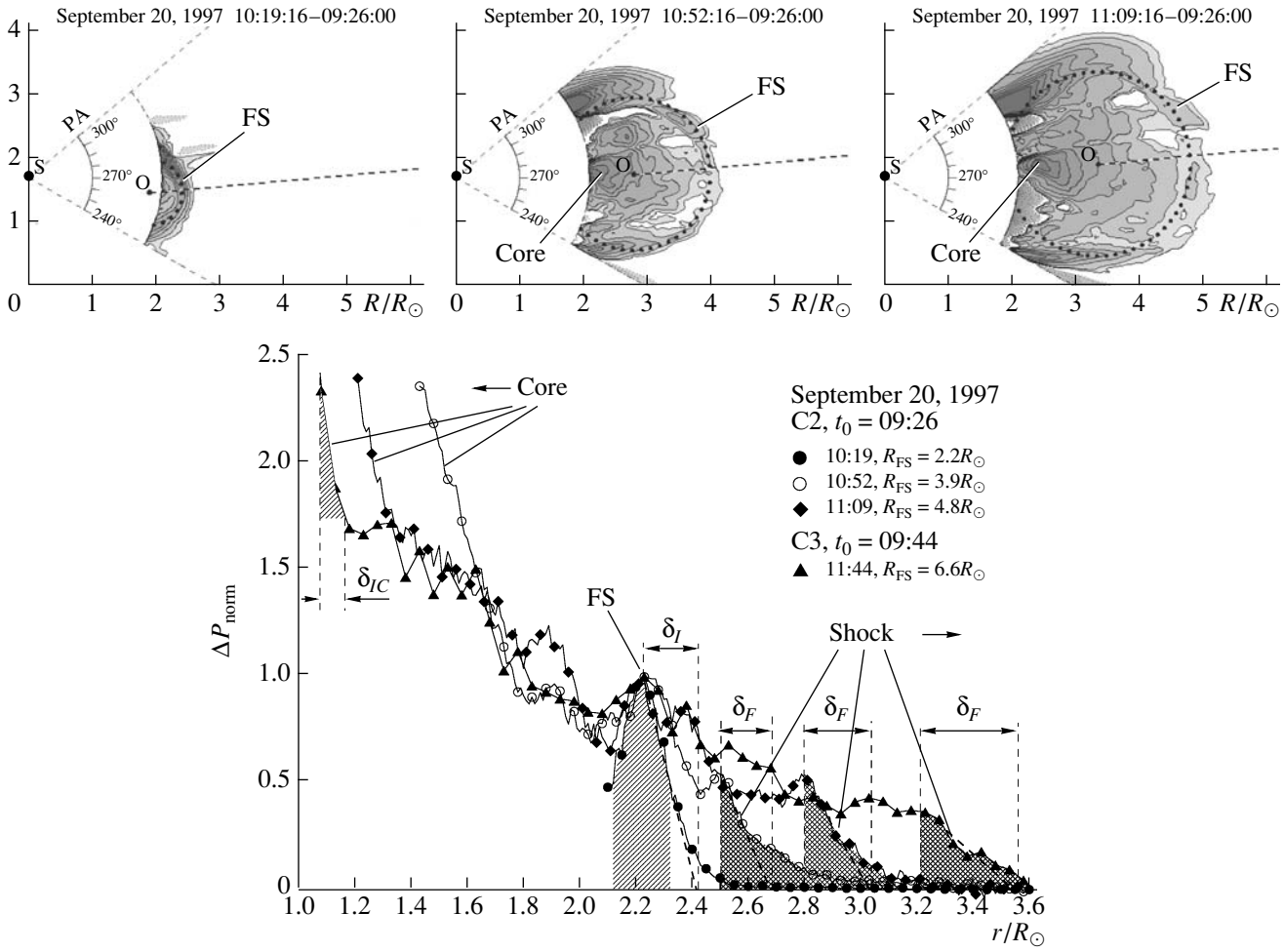

Fig. 2. CME observed on September 20, 1997, with the shock formation detected in the LASCO C2 and C3 data. The three upper plots present the differential brightness images for three particular times, while the lower plot shows the differential brightness distributions for successive times. The notation is the same as in Fig. 1.

$\rho_e \sim 10^{-9}\ R_\odot$ and $\tau_{ep} \sim 3$ s. From this estimate, we find that, over the time for the CME's propagation in the corona (several hours), the thickness of the current sheet remains below $\sim 100\rho_e$ ($\sim 10^{-7}\ R_\odot$), significantly below the spatial resolution of the Mark 4 and C2 coronagraphs, which is $K \approx 0.02\ R_\odot$. Thus, the minimum width of the current sheet detected should be at best near the spatial resolution of the instruments.

When the current sheet moves as a whole, a perturbed region in front of the sheet is formed due to the compression of the background plasma and the excitation of oscillations in the plasma density and magnetic field. In this case, the jump in brightness in the current-sheet image will be enlarged due to the contribution of the perturbed zone.

The jump in brightness at the shock front is also associated with the density irregularity on the scale of the front. However, this jump differs from the current-sheet jump, since there is a retardation and heating of the supersonic flow at the shock front. Since the shock front moves with supersonic velocity relative to the surrounding medium, there are no perturbations and no perturbed zones preceding the shock front. Therefore, the shock front undergoes no distortion, in contrast to the perturbed zones preceding moving current sheets.

Note that the visible size of both a stationary current sheet and a shock front can exceed their true sizes, due to the additional brightness contributions of some coronal regions that are not connected with but are projected onto the density jump along the line of sight.

Thus, we can approximately estimate the thickness of the current sheet from the size of the brightness jump in the image. At the boundary of the frontal structure, the width of the current sheet is defined as

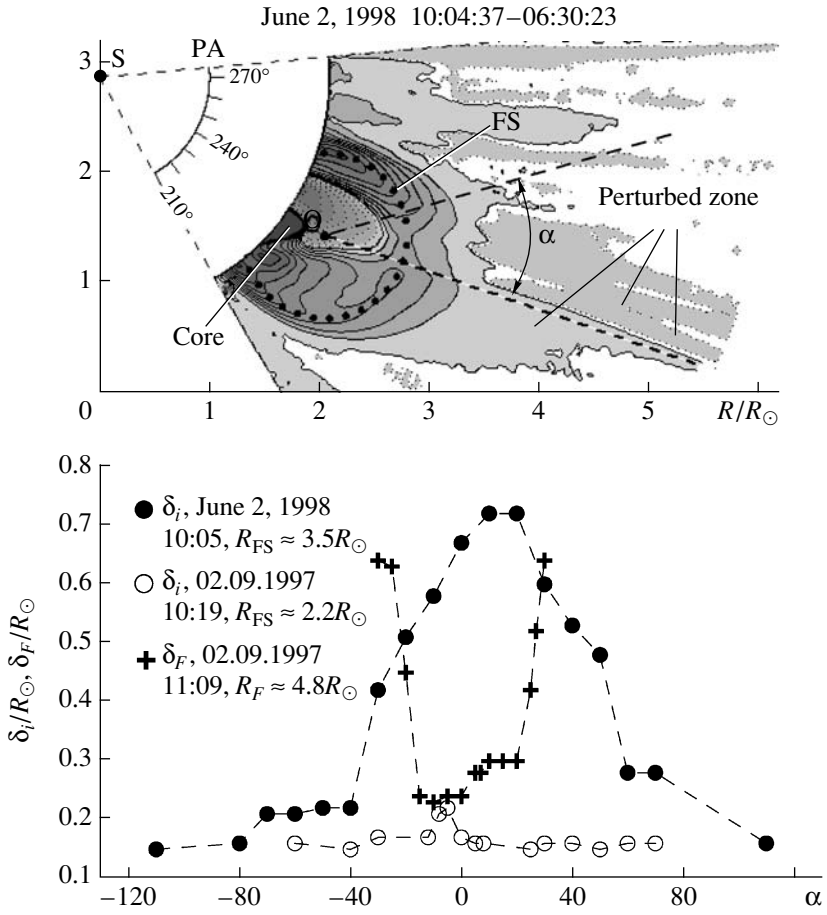

Fig. 3. Top: contours of the differential brightness for the CME observed on June 2, 1998 at 10:04. Bottom: visible width of the brightness jump as a function of the angle α measured from the direction of propagation of the CME, at the boundary of the CME frontal structure observed on June 2, 1998 at 10:05 (filled circles) and September 20, 1997 at 10:19 (hollow circles), as well as at the boundary of the CME shock front observed on September 20, 1997 at 11:44 (pluses).

twice the brightness jump detected at half its height (δ_I in the lower plot of Fig. 2). In addition, we can determine the width δ_{IC} of the current sheet located at the boundary of the core containing dense material from the erupting filament. In Fig. 2, this thickness is shown only provisionally, because the maximum core brightness, which is actually much higher, has been restricted in this plot. Figure 2 illustrates the width of the shock front in the same way, where the brightness jump has a characteristic size of δ_F.

In order to understand the difference between the current sheet and the shock, let us consider the CME observed on June 2, 1998 (first appearance at 08:08, PA $\approx 245°$, $V \approx 751$ km/s). In this event, in contrast to the event of September 20, 1997, the velocity was below the critical value, and no shock was observed, at least in the C2 field of view (i.e., closer than $\approx 6\ R_\odot$). The upper plot of Fig. 3 presents contours of the differential brightness for this event at 10:04. Similarly to the ejections discussed above, we can see here three individual CME parts (frontal structure, cavity, and core) and an extended perturbed zone preceding the CME.

If we take the frontal structure to have the form of a circular arc, we can determine the size of the current sheet at the leading boundary of the frontal structure in various directions. Sections of the differential brightness were constructed from the center of the frontal structure and used to determine the size of the current sheet δ_I. The position of each section was determined by the angle α from the center of the frontal structure, measured from the direction of the CME propagation, with α being positive in the counterclockwise direction.

The filled circles in the lower plot of Fig. 3 show the thickness of the current sheet at the boundary of the frontal structure δ_I as a function of the angle α for the CME observed on June 2, 1998 at the time indicated in the upper plot. At this time (10:05, the maximum distance to the frontal structure is $R_{FS} \approx 3.5R_\odot$), there is a well pronounced perturbed zone preceding the frontal structure. Owing to this zone, δ_I in the

direction of the CME propagation ($\alpha \approx 0°$) exceeds δ_I for lateral directions ($\alpha \approx \pm 100°$) by almost a factor of five. For the CME observed on September 20, 1997 at 10:19 (the maximum distance of the frontal structure from the center of the Sun reaches $R_{\rm FS} \approx 2.2 R_\odot$), the shock front is not yet detected, and we can also determine δ_I for various angles α (hollow circles in the lower plot of Fig. 3). The thickness δ_I is approximately constant, 0.15 $R_\odot$, and is about twice as large only in the direction of the CME propagation ($\alpha \approx 0°$).

Thus, the appearance of the perturbed zone seems to result in an increase in the visible thickness δ_I. For larger angles α (in lateral directions), the perturbed zone is weak and δ_I takes its minimum.

We can construct a similar dependence on the angle α for the thickness of the shock front. The pluses in the lower plot of Fig. 3 show the function $\delta_F(\alpha)$ for the CME observed on September 20, 1997 at 11:09, when the maximum distance to the shock front reaches $R_F \approx 4.8\ R_\odot$. It is obvious that $\delta_F(\alpha)$ differs from the function $\delta_I(\alpha)$. One reason for this could be the absence of a perturbed zone preceding the shock front. In this case, the thickness of the shock front may depend on local parameters of the surrounding plasma, as well as the velocity normal to the shock front (which decreases with α), which could result in a change in the type of the shock.

5. ESTIMATE OF THE RESOLUTION

Can we identify the increase in the visible thickness of the current sheet due to the effect of the perturbed zone, and determine the maximum spatial resolution provided by the instruments available? This question can be formulated as follows: what is the minimum width of a current sheet in the corona that we can detect with the Mark 4 and LASCO C2 instruments?

In addition to the effect of the perturbed zone, a visible increase in the thickness of the current sheet can occur due to the total influence of irregularities in the sheet projected onto the line of sight. The longer an irregular section, the stronger this increase can be. Therefore, this increase is minimum for a current sheet whose minimum size is observed along the line of sight. One example is the boundary of an erupting filament in the form of the thin loop with a small size observed along the line of sight.

The upper left plot of Fig. 4 shows the differential polarized brightness detected by the Mark 4 instrument for the CME that began on the Western limb on June 28, 2000 at 19:00. This event displayed a filament eruption, which was clearly visible in both the Mark 4 and LASCO C2 images (higher in the corona, in the latter case). This enables us to compare the Mark 4 and LASCO C2 resolutions. We used differential-brightness profiles across the filament loop along the dashed line passing through the filament center (upper left plot in Fig. 4). This direction (lateral to the filament eruption) was used to minimize the effect of the perturbed zone, which arises mainly in the direction of motion. Profiles of the differential brightness constructed with the Mark 4 and C2 data were normalized to the maximum brightness and shifted to match their maxima (upper right plot shown in Fig. 4). The spatial size of the brightness jump at the filament boundary remains nearly constant, reaching $\delta_{IC} \approx 0.045\ R_\odot$ for all distances from $R \approx 1.3\ R_\odot$ to $R \approx 6.1\ R_\odot$. This approaches the spatial resolution of the Mark 4 and C2 instruments ($K \approx 0.02\ R_\odot$). Given other factors affecting the images (in particular smearing of moving elements in the image due to the finite exposition time), we find this agreement to be satisfactory. The profile of the brightness jump is somewhat broadened at $R \approx 6.1\ R_\odot$ (hollow triangles in the upper right plot of Fig. 4), probably due to the effect of the perturbed zone, which becomes stronger at greater distances.

In some cases, the minimum width of the jump can be observed in the current sheet located at the boundary of the CME frontal structure. The lower left plot of Fig. 4 presents the CME observed on the Western limb on April 7, 2001 (which began at about 17:00). The filled circles in the lower right plot of Fig. 4 show the normalized brightness profile observed at the boundary of the frontal structure in lateral directions, where the effect of the perturbed zone is minimum. This plot is combined with the brightness profile observed at the filament boundary at nearly the same distance on June 28, 2000 (hollow circles in the lower right plot of Fig. 4). It is obvious that the thickness of the current sheet located at the boundary of the fairly long frontal structure extended along the line of sight differs negligibly from the thickness of the current sheet located at the boundary of the comparatively thin (along the line of sight) filament.

Thus, the minimum width of the brightness jump detected by the Mark 4 and LASCO C2 coronagraphs is approximately 0.045 $R_\odot$, and this width approaches the spatial resolution ($K \approx 0.02\ R_\odot$) of these instruments. The perturbed zone apparently makes the main contribution to the enlargement of the jump width. Therefore, we can assume that the observed width of the shock front ($\delta_F \approx 0.2\ R_\odot$ shown in the lower plot of Fig. 2) describes its real size, since any perturbations preceding the shock front should be absent, and the detected width of the front considerably exceeds the spatial resolution of the instrument. Calculations carried out for a simple geomet-

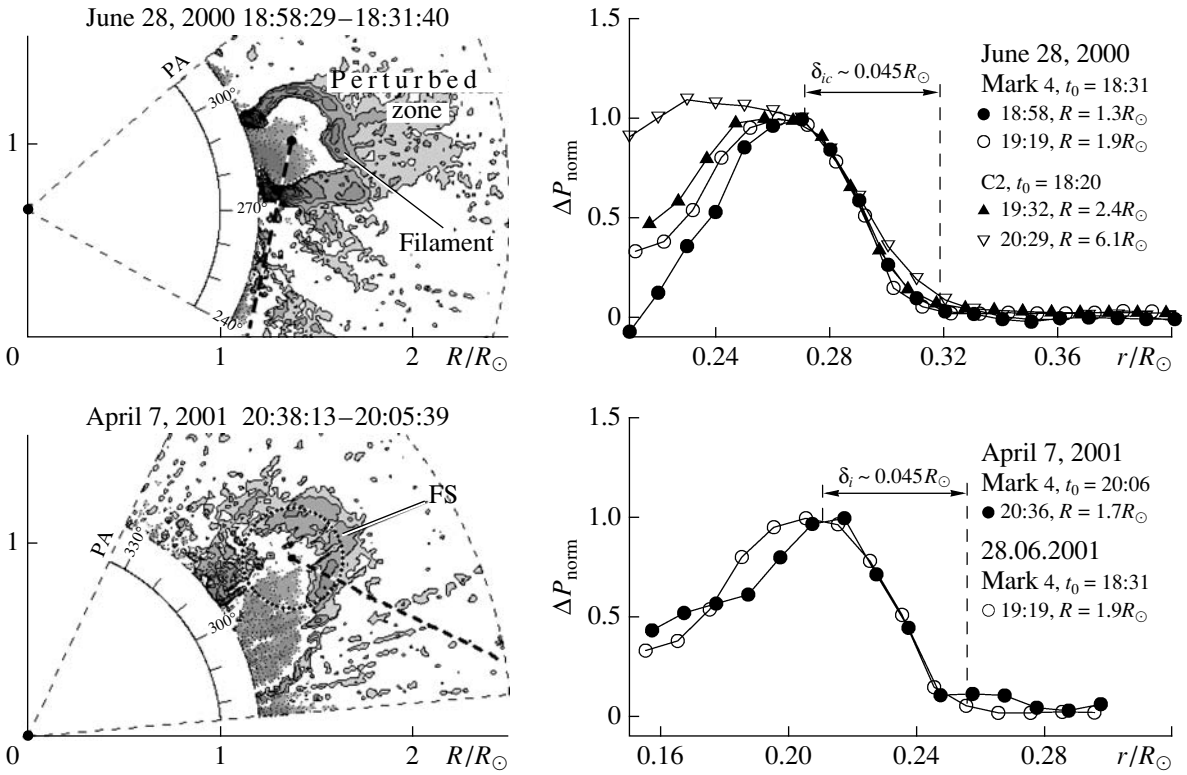

Fig. 4. Left: differential brightness for the two CMEs observed on June 28, 2000 with a filament eruption (top) and April 7, 2001 with a visible frontal structure (bottom). Right: comparison of differential-brightness profiles across the filament at various distances for the event observed on June 28, 2000 (top) and across the frontal structure for the event observed on April 7, 2001 (bottom). The Mark 4 and LASCO C2 data were used.

rical model with a quasi-spherical shock show that the observed width δ_F of the brightness profile approaches the width δ_N of the density jump occurring in the shock [10].

6. DISCUSSION OF THE ENERGY DISSIPATION IN THE SHOCK

The size of the front δ_F enables us to draw some conclusions on the energy dissipation in the shock. The first question that must be answered is whether the dissipation is collisionless [14] or collisional [15].

Collisionless dissipation is determined by collective processes excited by some plasma instabilities. In magnetized plasmas, the maximum front widths are displayed by quasi-parallel shocks, and do not exceed [16]

$$\delta_1 \approx (10 - 100)\rho_p,$$

where ρ_p is the Larmor radius of protons for the unperturbed magnetic field B immediately preceding the front. In rarefied plasmas without magnetic fields, the maximum front width is determined by the ion–ion two-stream instability, and does not exceed [17, 18]

$$\delta_2 \approx 100 r_D,$$

where r_D is the Debye radius.

Let us estimate these quantities for the plasma of the streamer belt assuming, for example, the temperatures $T_e \approx T_p \approx 10^6$ K and density $N \approx 5 \times 10^5$ cm^{-3} at the distance $R = 3.5\ R_\odot$ [19]. We adopt a magnetic field $B \approx 5$ G at the solar surface and assume a quadratic decrease in the magnetic field with distance in the corona, so that $B \approx 5\ \mathrm{G} \times (R_\odot/R)^2 \approx 0.4$ G. To estimate the Larmor radius, we assume a proton velocity $V = 3 \times 10^3$ km/s for the most rapid ejections. Thus, we obtain $\delta_1 \approx 100\rho_e \sim 10^{-4}\ R_\odot \ll \delta_F$ and $\delta_2 \approx 100 r_D \sim 10^{-8}\ R_\odot \ll \delta_F$. It is quite clear that the front width for a collisionless shock is much smaller than the resolution limit of all known coronagraphs. In this case, the visible front size is determined by the instrument resolution. However, the measurements show that the front width is much larger than this limit, at least at distances $R < 5\ R_\odot$ in the streamer belt. Therefore, we conclude that the energy dissipation is collisional at these distances. In this case, the energy dissipation in the shock must occur on length scales approaching the mean free path of protons λ_p, and this scale should determine the front width δ_F [15].

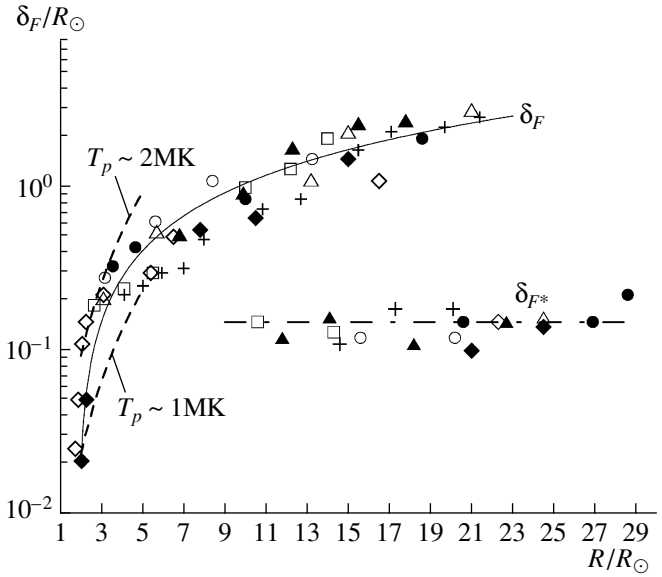

Fig. 5. Front widths of collisional δ_F and collisionless δ_F^* shocks as functions of the distance R from the center of the Sun for eight CMEs with high velocities observed on June 11, 1998 (filled circles, PA = 80°), March 3, 2000 (pluses, PA = 230°), June 28, 2000 (filled triangles, PA = 270°), September 4, 2000 (hollow squares, PA = 300°), April 21, 2002 (hollow triangles, PA = 270°), November 4, 2003 (hollow circles, PA = 238°), November 22, 2001 (filled diamonds, PA = 247°–254°), and October 26, 2003 (hollow diamonds, PA = 265°–290°) with the Mark 4, LASCO C2 and LASCA C3 instruments. The dashed curves show the mean free paths of protons calculated for temperatures of 1 and 2 MK.

The mean free path of protons in solar radii is

$$\lambda_p \approx 10^{-7} T^2/N. \quad (1)$$

Here, T and N are the temperature (in K) and density (in cm^{-3}) of the protons in the unperturbed plasma immediately preceding the shock front.

Let us compare the visible front width δ_F with λ_p in the corona. For this purpose, we used the SOHO/UVCS and LASCO proton temperature and electron-density measurements carried out in the region of the equatorial streamer [19]. Let us assume that the proton temperature and plasma density within (2–5 $R_\odot$) follow Figs. 3a and 3c in [19]. The mean free path calculated using (1) then takes the form shown by the upper dashed curve in Fig. 5. The increase in λ_p with distance is due to the decrease in density, although this increase is limited by the weak decrease in temperature, with the mean free path being proportional to the temperature squared. The proton temperature detected in the corona somewhat exceeds the electron temperature; the difference is higher for heavier ions, which is attributed to additional ion-cyclotron heating [20]. When estimating the mean free path, we admit a significant error if we use an incorrect temperature. The lower dashed curve in Fig. 5 shows the calculated λ_p for the same density [19], but half the temperature detected (≈1 MK at 2 $R_\odot$), for the same decrease with distance. Note that a similar decrease with distance was found in [21] for measurements of the electron temperature carried out at $(1-1.3)$ $R_\odot$. The two dashed curves determine lower and upper limits for the mean free path of protons, depending on the temperature used.

Experimental dependences $\delta_F(R)$ were constructed using measurements of shock-front widths observed in the region of the streamer belt for eight CMEs with velocities $u > u_C$ detected at various distances. The corresponding shock-front-width measurements are presented in Fig. 5 by various symbols (along the solid curve marked δ_F). The solid curve shows the general behavior of the dependence, and represents a linearly approximation to the experimental data. The front width δ_F increases with distance. The characteristic scale of the front is comparable to the mean free path ($\delta_F \sim \lambda_p$), at least within ~5 $R_\odot$. This provides evidence for collisional energy dissipation in the shocks observed at these distances.

Returning to the lower plot in Fig. 3, which shows the width of the shock front δ_F as a function of the angle α measured relative to the direction of the CME propagation (the curve with pluses), we can assume that this function describes the distribution of the parameters of the medium through which the ejection passes. In the direction of the CME propagation ($\alpha \approx 0°$) is the streamer belt, which has a high density. With increase in the angle α, coronal sectors of lower densities (and consequently longer mean free paths λ_p) appear in front of the shock, which can result in

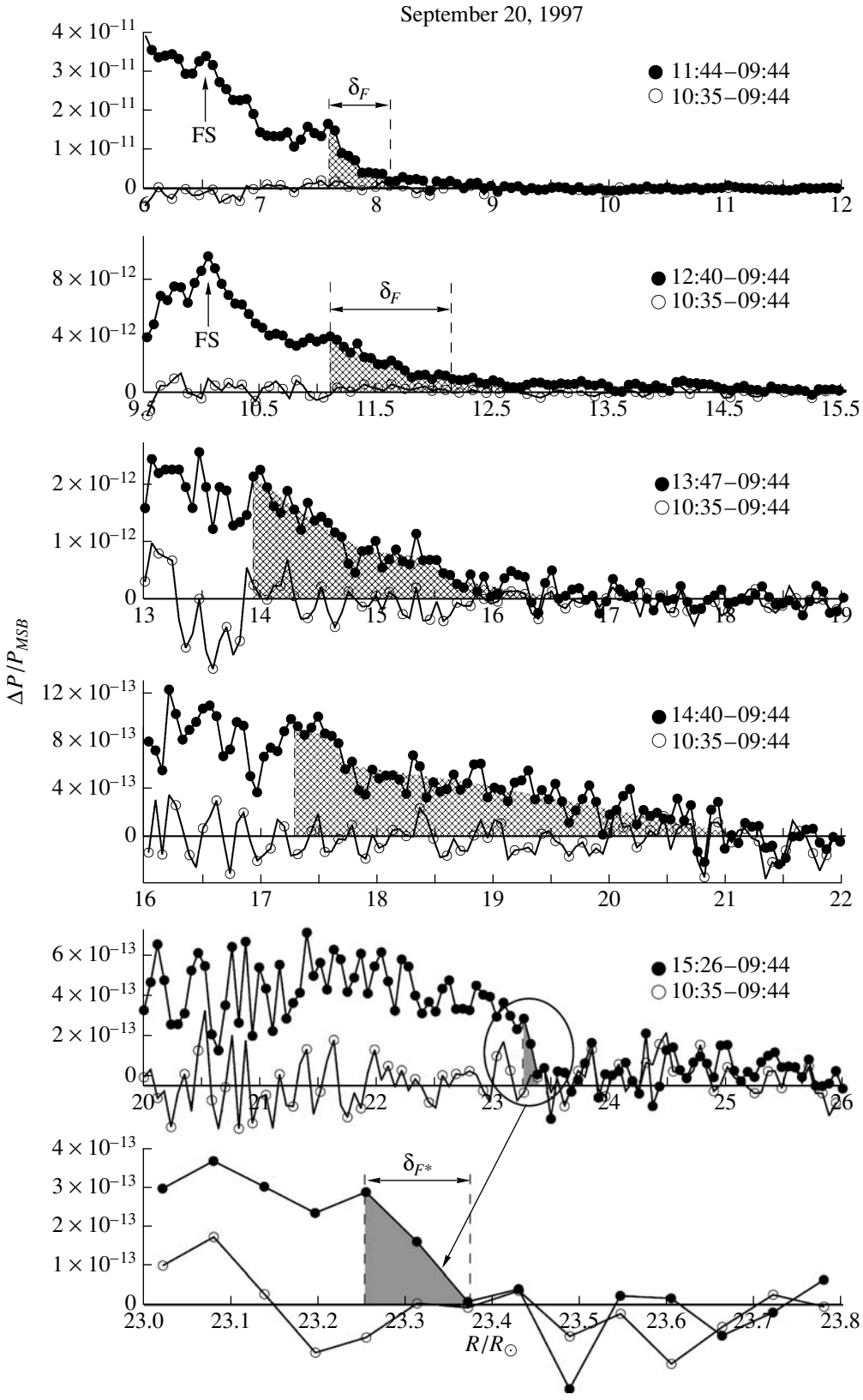

Fig. 6. CME differential brightness for distances exceeding 6 $R_\odot$ observed on September 20, 1997 at various times (filled circles). The unperturbed differential brightness (hollow circles) constructed for the time immediately preceding the CME can estimate the noise level.

different conditions for the shock excitation, down to the absence of the shock.

Thus, we are apparently dealing with a rare situation when we can experimentally resolve and examine shock fronts in plasma. Such attempts had failed for both gases and plasmas due to their extremely short λ_p values.

7. THE TRANSITION FROM COLLISIONAL TO COLLISIONLESS SHOCKS

The measured width of the shock front δ_F increases with the distance from the Sun. However, measurements carried out in situ in interplanetary space and near the Earth show that shocks detected at the fronts of interplanetary coronal ejections display very small widths $\delta_F^* \ll \lambda_p$, i.e. these shocks are collisionless. It is obvious that the shocks must make a transition from collisional to collisionless at some distance from the Sun. Apparently, we can observe this transition in the solar corona within the field of vision of the LASCO C3 coronagraph, at distances of less than 30 $R_\odot$ from the Sun.

Let us consider the shock behavior for the event of September 20, 1997 at $R > 6$ $R_\odot$. The filled circles in Fig. 6 show the differential brightnesses $\Delta P(t, R)$ constructed along the direction of the propagation of the CME (PA $= 270°-280°$) for successive times. These distributions continue the plots presented in the bottom of Fig. 2 to longer distances from the Sun; they are not normalized to the amplitude of the frontal structure or related to its position. The hollow circles show the differential brightnesses constructed for 10:35, immediately preceding the CME. These distributions can be used to estimate the noise at various distances, with the relative weight of this noise increasing with distance from the Sun. The fronts of collisional shocks are shown by crossed hatching in the brightness profiles. The width of the front δ_F increases with the distance R in accordance with the plot shown in Fig. 5, i.e., the front becomes broadened and smeared. Starting from $R \leq 20$ $R_\odot$, the formation of a new discontinuity occurs, which has a width $\delta_F^* \approx 0.15$ $R_\odot$ at $R \approx 23$ $R_\odot$.

The formation of a discontinuity with width $\delta_F^* \ll \lambda_p$ observed at distances 10 $R_\odot \leq R \leq 30$ $R_\odot$ has been detected for all eight CMEs whose measurements were used to construct the $\delta_F(R)$ plot shown in Fig. 5. The widths of discontinuities observed for various events are shown in Fig. 5 using the same symbols as δ_F, but these widths are marked δ_F^* (along the horizontal dot-dashed line). We can see that $\delta_F^* \approx (0.1-0.2)$ $R_\odot$ within the errors, independent of distance (dot-dashed line in Fig. 5). The discontinuity displays low amplitudes at the start of its formation and coexists with the collisional shock of width δ_F. The discontinuity amplitude gradually increases with distance, while the brightness profile behind the discontinuity flattens. Thus, the front makes a transition from the width δ_F to $\delta_F^* \ll \delta_F$.

The spatial resolution of the C3 instrument is $K \approx 0.12$ $R_\odot$, approximately equal to the visible width δ_F^* of the discontinuity. The true scale of the discontinuity could be much shorter than the visible scale, since the true scale remains unresolved in the coronal images. Together with the fact that δ_F^* does not change with distance, this supports the hypothesis that the discontinuity observed is a collisionless shock, whose width remains unresolved and limited by the spatial resolution of the C3 coronagraph. Note that such discontinuities in the brightness profiles preceding CMEs have been detected in rapid ($V > 1500$ km/s) CME halos [8]. The distance from the center of the Sun to the discontinuity exceeded 10 $R_\odot$. Those discontinuities were also associated with collisionless shocks.

The spatial sizes of the CME, the perturbed zone, and the shock increase with distance from the Sun R. Consequently, their effective sizes along the line of sight also increase. We expect that the resolution of the shock front decreases with R due to averaging along the line of sight. Nevertheless, we observed a front width nearing the coronagraph resolution in the LASCO C3 field of vision within distances $\geq$10 $R_\odot$; averaging along the line of sight apparently does not affect the measurements of the front width. This again supports the idea that the front width δ_F measured at shorter distances is nearly the true width, and the function $\delta_F(R)$ presented in Fig. 5 describes real changes in the front width with changing distance.

8. CONCLUSIONS

We have studied the perturbed zones and shocks preceding CMEs using data obtained with the Mark 4, LASCO C2, and C3 coronagraphs. The perturbed zone indicating the presence or absence of the shock is best observed in a frame moving with the CME frontal structure. The correctness of measurements of the width of the shock front δ_F using the Mark 4 and LASCO C2 data is supported. At distances $R < 5$ $R_\odot$ from the center of the Sun, the width of the shock front δ_F detected along the streamer belt is of the order of the mean free path of protons. This indicates that the energy dissipation in the shock front is collisional at such distances. At distances $R \geq (10-15)$ $R_\odot$, the formation of a new discontinuity with width $\delta_F^* \ll \delta_F$ is observed in the leading portion of the shock front. Within the errors, $\delta_F^* \approx (0.1-0.2)$ $R_\odot$; this width is independent of the distance R and is limited by the spatial resolution of the LASCO C3 instrument. The discontinuity on the

scale δ_F^* displays low amplitudes at the start of its formation and initially coexists with the shock front of width δ_F. The relative amplitude of the discontinuity gradually increases with distance, while the brightness profile flattens behind it. These changes are interpreted as a transition from a collisional to a collisionless shock.

ACKNOWLEDGMENTS

The author is grateful to the Naval Research Laboratory (USA), Max Planck Institute of Aeronomy (Germany), Space Astronomy Laboratory (France), and University of Birmingham (UK) for the SOHO/LASCO data used. The Mark 4 data were provided by the Mauna Loa Solar Observatory (http://mlso.hao.ucar.edu/). This work was supported by the Program P-16 of the Presidium of the Russian Academy of Sciences, the Program of State Support for Leading Scientific Schools of the Russian Federation (NSh-2258.2008.2), and the Russian Foundation for Basic Research (project code 09-02-00165a).

REFERENCES

1. N. Gopalswamy, W. T. Thompson, J. M. Davila, et al., Solar Phys. **259**, 227 (2009).
2. J. C. Raymond, B. J. Thompson, O. C. St. Cyr, et al., Geophys. Res. Lett. **27**, 1439 (2000).
3. S. Mancuso, J. C. Raymond, J. Kohl, et al., Astron. Astrophys. **383**, 267 (2002).
4. A. Ciaravella, J. C. Raymond, S. W. Kahler, et al., Astrophys. J. **621**, 1121 (2005).
5. A. Vourlidas and V. Ontiveros, arXiv:0908.1996v1 [astro-ph] (2009).
6. A. Vourlidas, S. T. Wu, A. H. Wang, et al., Astrophys. J. **598**, 1392 (2003).
7. W. B. Manchester IV, A. Vourlidas, G. Toth, et al., Astrophys. J. **684**, 1448 (2008).
8. V. Ontiveros and A. Vourlidas, Astrophys. J. **693**, 267 (2009).
9. M. Eselevich and V. Eselevich, Astron. Zh. **84**, 1046 (2007) [Astron. Zh. **51**, 947 (2007)].
10. M. Eselevich and V. Eselevich, Geophys. Res. Lett. **35**, L22105 (2008).
11. G. E. Brueckner, R. A. Howard, M. J. Koomen, et al., Solar Phys. **162**, 357 (1995).
12. L. A. Artsimovich, *Controlled Thermonuclear Reactions* (Gos. Izd-vo Fiz.-Mat. Lit-ry, Moscow, 1961; Gordon and Breach, New York, 1964).
13. G. Mann, A. K. Klassen, C. Estel, et al., in *Proc. 8th SOHO Workshop: Plasma Dynamics and Diagnostics in the Solar Transition Region and Corona*, Ed. by J.-C. Vial and B. Kaldeich-Schumann, ESA Spec. Publ., SP-446 (ESA, 1999), p. 477.
14. R. Z. Sagdeev, in *Problems of Plasma Theory*, Collected vol., No. 2 (Gosatomizdat, Moscow, 1964), p. 20 [in Russian].
15. Ya. B. Zel'dovich and Yu. P. Raizer, *Elements of Gas Dynamics and the Classical Theory of Shock Waves* (Nauka, Moscow, 1966; Academic, New York, 1968).
16. V. G. Eselevich, Planet. Space Sci. **6**, 615 (1983).
17. D. A. Tidman, Phys. Fluids **10**, 547 (1967).
18. O. L. Volkov, V. G. Eselevich, G. N. Kichigin, and V. L. Papernyi, Zh. Eksp. Teor. Fiz. **67**, 1689 (1974) [Sov. Phys. JETP **40**, 841 (1974)].
19. L. Strachan, R. Suleiman, A. V. Panasyuk, et al., Astrophys. J. **571**, 1008 (2002).
20. E. Marsh, in *The 31st ESLAB Symposium on Correlated Phenomena at the Sun, in the Heliosphere, and in Geospace* (Eur. Space Agency, Noordwijk, Netherlands, 1997), p. 7.
21. C. David, A. H. Gabriel, and F. Bely-Dubau, in *Proc. 5th SOHO Workshop: The Corona and Solar Wind*, Ed. by A. Wilson, ESA Spec. Publ., SP-404 (ESA, 1997), p. 319.

Translated by V. Badin